Multimodal assessment of the curing of agglomerated ores in the presence of chloride ions

Luis Salinas-Farran[a*], Andrew Batchelor[b], Stephen J. Neethling[a]

[a] Department of Earth Science and Engineering, Imperial College London, London, SW7 2AZ, United Kingdom

[b] Faculty of Engineering, University of Nottingham, University Park, Nottingham, NG7 2RD, United Kingdom

Abstract

Agglomeration and subsequent curing are widely used as pre-treatment for ore prior to heap leaching as both improve the permeability of the heap and bring leaching solution into close contact with the ore, initializing the leaching reactions. Despite its widespread use there have been limited studies into the processes occurring within the agglomerates over the curing process. In this study both destructive and non-destructive imaging techniques are used to assess both the physical and chemical changes occurring within the agglomerates as they cure.

The SEM/EDX is one of the most popular imaging techniques for mineral samples. It can only be carried out once for a given sample due to its destructive preparation method but provides detailed mineralogical information. A complementary tool is X-ray Microtomography (XMT), which is non-destructive and can be used to image the same object multiple times over the course of the experiment. Its main limitation, though, is that the acquired images are of X-ray attenuation values and need to be independently assigned to different mineral classifications based on, for instance, the corresponding SEM images. Combining the ability of SEM/EDX measurements to identify different mineral phases with the 3D time resolved XMT measurements can thus produce superior results to those achievable using either of the modalities on their own.

In this study, we propose a methodology for quantifying the formation and depletion of mineral components of agglomerate. These methodologies will be demonstrated in ores agglomerated using a combination of sulphuric acid and ferric sulphate as well as in samples in which sodium chloride is added to the agglomeration recipe. The curing process was tracked beyond the typical time scales used industrially, highlighting that the presence of chloride ions makes a substantial difference to the chemical and structural evolution of the sample. Over this curing process most of the observed leaching occurs during the first 20 days in the presence of NaCl, while there is virtually no metal dissolution for the standard samples without NaCl. During curing the solution does not leave the agglomerates other than via evaporation. Thus, reprecipitation of metal containing mineral species was observed, especially near the agglomerate surfaces. In the presence of NaCl precipitated Cu-S-O-Cl complexes were observed suggesting that the chloride ions in solution are playing a key role in the leaching process. After 65 days of curing, the samples were water washed in order to remove soluble species, extracting 50% of the original sulphides from the agglomerates containing sodium chloride, but only 20% from the other agglomerates.

1. Introduction

Key parameters in heap leaching include permeability, mechanical stability, and mass transport. All of these properties can be manipulated by performing agglomeration as an intermediate step between crushing and stacking the ores into heaps. After contacting the ore with an agglomeration solution and producing agglomerates using a pan or drum agglomerator, a subsequent curing period is often carried out prior to irrigating the pile with the leach solution. While the primary purpose of curing is usually to develop the mechanical strength of the agglomerate, it is also during this process that a first chemical attack on the minerals occurs, kickstarting the leaching reactions. It is thus essential to understand the impact of both the chemical composition of the agglomeration solution and the length of the curing process on the overall leaching performance.

1.1. Agglomeration solution

While most of the heap leaching literature has focused on the active leaching stage, there is evidence that promoting leaching reactions during the agglomeration and curing stage can enhance the overall performance of the heap leaching process (Lu, Dreisinger and West-Sells, 2017). It is thus common to use a mixture of acidic solution or raffinate and other chemical reagents as the agglomeration solution in order to enhance metal dissolution during the curing process.

Due to the refractory nature of sulphides, an oxidizing agent is necessary to maintain the appropriate redox conditions and thus successfully accomplish metal dissolution. Sulphides also frequently exhibit slow leaching kinetics, thus chemical reagents that enhance leaching performance are added to the agglomeration solution. Ferric ions are commonly added as an oxidizing agent, e.g. reaction (1), in to order to enhance the leaching that occurs during curing. Oxygen can also act as an oxidizing agent in the leaching process, e.g. reaction (2), although it is harder to maintain an oxygen flow over the curing process. It is worth noting that equations (1) and (2) represent the oxidative dissolution of chalcopyrite in sulphuric acid media.

$$CuFeS_{2(s)} + 4Fe^{3+}{}_{(aq)} \rightarrow Cu^{2+}{}_{(aq)} + 5Fe^{2+}{}_{(aq)} + 2S^{0}{}_{(s)} \quad (1)$$

$$CuFeS_{2(s)} + O_{2(g)} + 4H^{+}{}_{(aq)} \rightarrow Cu^{2+}{}_{(aq)} + Fe^{2+}{}_{(aq)} + 2S^{0}{}_{(s)} + 2H_2O_{(aq)} \quad (2)$$

Chalcopyrite dissolution at ambient temperature has been shown to have a higher reaction rate in a chloride/chloride-sulphuric media than that achieved using only a sulphuric media. This is because in the presence of chloride ions, the passivation layer formed by the elemental sulphur in reactions (1) and (2) becomes more porous and crystalline, permitting reactions to proceed (Lu, Jeffrey and Lawson, 2000a, 2000b; Carneiro and Leão, 2007; Ghorbani, Franzidis and Petersen, 2016). Furthermore, Cu^{+} is stable in chloride media, allowing the use of both Cu^{2+} and Fe^{3+} as oxidant ions for the dissolution reaction (Yévenes *et al*., 2010) as shown by equations (3), (4), and (5). The exact reaction mechanism depends on the chemistry and leaching conditions. Mixed-potential electrochemical models are commonly used to describe the dissolution of chalcopyrite in both chloride and sulphate media, although experimental data has shown that an extended reaction model in which chalcopyrite partially dissolves non-oxidatively provides a more consistent alternative (Nicol *et al.*, 2010). Yet, the reaction pathway is still a matter for debate (Liddicoat and Dreisinger, 2007; Yoo *et al.*, 2010; Veloso *et al.*, 2016; Bobadilla-Fazzini *et al.*, 2017).

$$CuFeS_{2(s)} + 3FeCl_{3(aq)} \rightarrow CuCl_{(aq)} + 4FeCl_{2(aq)} + 2S^{0}{}_{(s)} \quad (3)$$

$$CuFeS_{2(s)} + 4FeCl_{3(aq)} \rightarrow CuCl_{2(aq)} + 5FeCl_{2(aq)} + 2S^{0}{}_{(s)} \quad (4)$$

$$CuFeS_{2(s)} + 3CuCl_{2(aq)} \rightarrow 4CuCl_{(aq)} + FeCl_{2(aq)} + 2S^{0}{}_{(s)} \quad (5)$$

1.2. Curing time

During the curing stage agglomerates dry out, and cementation reactions occur. Moreover, since the agglomeration solution contains leaching agents, there will be metal dissolution. Much of the dissolved metals will reprecipitate due to the saturation of the solutions brought about by the evaporation of the moisture (Purkiss and Anthony, 2002).

The length of the curing process is a critical variable to control, though the optimum curing time will depend on both the mineralogical characteristics of the ore, as well as on the reagents added to the agglomeration solution. A number of researchers have demonstrated that an extended curing period will enhance metal recovery (Cerda *et al.*, 2018; Media *et al.*, 2018; Quezada *et al.*, 2018; Velásquez-Yévenes *et al.*, 2018; Hernández *et al.*, 2019). This paper will extend the previous work by investigating the agglomerate and grain scale processes occurring during the curing process and, in particular, the difference in behaviour with and without the presence of chloride ions. This will involve applying a ranging of imaging and image analysis techniques in order to track the evolution of the distribution of metal species in both the mineral grains and subsequent precipitates, as well as the agglomerate structure.

There has been a few investigations on the structural evolution of agglomerates over the curing process. This might be due to the destructive nature of common imaging techniques, such as Energy-dispersive X-rays (EDX) in a Scanning Electron Microscope (SEM), commonly used together with automated

mineralogical analysis software packages[1]. As the sample preparation procedure involves destroying the sample, it makes it impossible to track structural changes over time. This work will thus combine the high resolution 2D mineralogical characterisation obtainable from SEM/EDX with the 3D time resolved imaging obtainable using X-ray Microtomography.

1.3. X-ray Microtomography (XMT) as a characterization tool

X-ray Microtomography (XMT) is an attractive complementary technique for sample characterization due to its non-destructive/non-invasive nature. The XMT technique allows the same sample to be periodically scanned, producing a time series of 3D representations of the scanned object. These images are based on variations in the X-ray attenuation of the material resulting in a range of grayscale values. The differences in histogram values permit the discrimination between the sample components, which for the copper-ore samples are pores, mineral grains, and rock matrix. Thus, the 3D XMT images can form the basis for both a qualitative and quantitative analysis of the agglomerate evolution, including both structural evolution and leaching behaviour.

The XMT based assessments have been widely used to quantify liberation (Miller *et al.*, 2009; Reyes *et al.*, 2018), structural changes (Kareh *et al.*, 2014; Ram *et al.*, 2020), preferential breakage (Garcia, Lin and Miller, 2009), and leaching extent (Lin, 2015; Lin *et al.*, 2016; Dobson *et al.*, 2017; Yang *et al.*, 2019) in mineral samples. A disadvantage of using XMT, though, is that different sulphides will present similar attenuation values when exposed to an X-ray beam. This means that for a typical mineral sample containing more than one type of metal sulphide (e.g. primary and secondary copper sulphides), it is very hard to quantify the dissolution rate of each component separately. This issue has been addressed before by calibrating the XMT measurements with two dimensional images containing more detailed mineralogical data (Gay and Morrison, 2006; Reyes *et al.*, 2017). The ability of the SEM/EDX measurements to identify different mineral phases can then be combined with 3D time resolved XMT measurements, therefore producing superior results to those achievable using either of the modalities on their own.

The purpose of this paper is thus to extend the knowledge on the chemical and structural evolution of agglomerated ores over the curing process by describing both grain dissolution and sulphide reprecipitation in 4D. For this purpose, a quantification methodology is presented using a combination of BSE/MLA and XMT for mineral characterization. This methodology takes advantage of the slightly different X-ray attenuation of the precipitating compounds, which allows them to be identified in the XMT images. This is important because, unlike during the heap leaching stage, all of the metal that is leached from the sulphide grains during curing remains in the agglomerate particles. Without the ability to distinguish between the original mineral grains and the precipitates it would be very challenging to quantify the rates of dissolution of grains as this can be obscured by material reprecipitating on their surfaces. In addition to the quantitative tracking of the dissolution and precipitation processes, the XMT images allows the evolution of the structure of the agglomerates to be tracked, including the formation of bridges between particles, the evolution of the pore spaces within the agglomerates, desiccation cracks and changes in the overall morphology of the agglomerates.

2. Experimental procedure

The mineral ore used in this study was obtained from Escondida mine, located in Antofagasta, northern Chile. Table 1 summarises the mineral composition as obtained from SEM assessment. Its copper grade is approximately 0.4%, with chalcopyrite being the main copper-containing mineral, and pyrite the primary sulphide component. The overall metal-sulphide grade was 3.7%, with a rock matrix mainly composed of quartz and clays.

[1] Automated mineralogical analysis software packages such as MLA or QEMSCAN; or more recent products, namely Zeiss Mineralogic, TESCAN TIMA, Oxford Instruments INCA Mineral.

Table 1. Main mineral species within the ore feed used for the agglomeration tests.

Mineral type	Weight (%)
Copper containing species	**0.83[a]**
Chalcopyrite	0.67
Chalcocite	0.11
Covellite	0.05
Pyrite	**2.82[a]**
Gangue minerals	**90.15[a]**
Quartz	19.81
Kaolinite	34.82
Illite	12.32
Muscovite	11.00
Montmorillonite	6.82
Alunite	5.21
Svanvergite	0.17
Other gangue minerals	**6.2[a]**

a.Indicates the totals for a category of mineral, with the individual minerals in the list.

2.1. Agglomeration tests

In order to produce agglomerates of industrial quality, agglomeration tests were conducted using a standard particle size distribution for the feed material, shown in Figure 1 (D_{80} of approximately 19 mm). Two different agglomeration solutions were tested, which contained Cu^{2+}, Fe^{2+}, Fe^{3+}, and trace metals Al and K added in the form of $CuSO_4 \bullet 5H_2O$, $FeSO_4$, $Fe_2(SO_4)_3 \bullet 4H_2O$, K_2SO_4, and Al, respectively. The chemical composition of the two agglomeration solutions is summarized in Table 2. The only difference between solutions A and B is that the first one contains chloride ions in the form of NaCl (approximately 150 g/L of Cl^-).

Agglomeration was performed by feeding the mineral ore jointly with the solution into a tumbling drum of 174 mm height and 127 mm diameter. The material had a residence time of 3 min inside the drum, which produced agglomerates with a D_{80} of approximately 25 mm. Lastly, two columns of 28 mm diameter and 190 mm height were filled with approximately 129 g of agglomerates. These were then placed within an incubator at a fixed temperature of 35°C. An extended curing time of 65 days was used in order to better understand the evolution of the agglomerates. Figure 2 shows the experimental rig including the incubator and the two columns. After the 65 days of curing, both columns were water-washed for 5 days in order to extract soluble species that had formed and reprecipitated during the curing process.

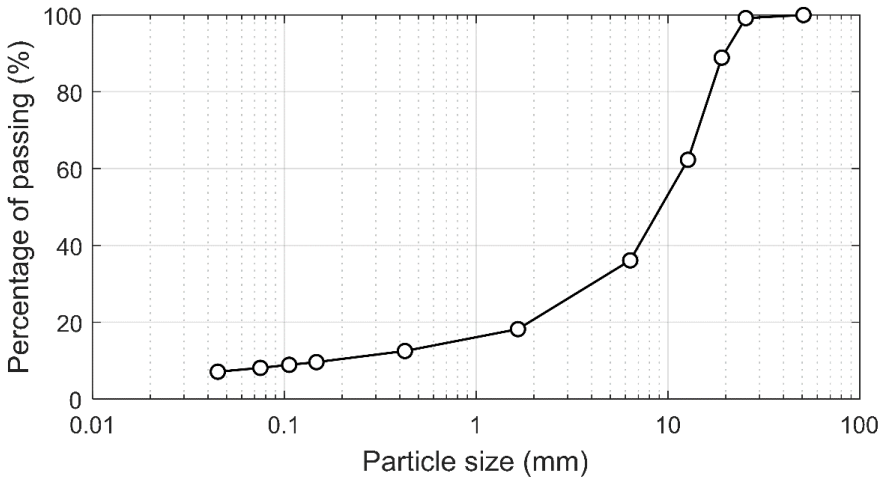

Figure 1. Particle size distribution of the feed material for agglomeration.

Table 2. Agglomeration conditions.

Agglomeration conditions		**Solution composition**	**(g/L)**
Mass of mineral (g)	728.50	**$CuSO_4 \bullet 5H_2O$**	1.40
H_2SO_4 (kg/t of mineral)	12	**$FeSO_4$**	4.35
Volume of solution (mL)	77.76	**$Fe_2(SO_4)_3 \bullet 4H_2O$**	6.73
Agglomeration time (min)	3	**NaCl**	0^B – 247.28^A
Fraction of the critical speed	0.30	**K_2SO_4**	1.03
		Al	7.00

A: corresponds to recipe A.
B: corresponds to recipe B.

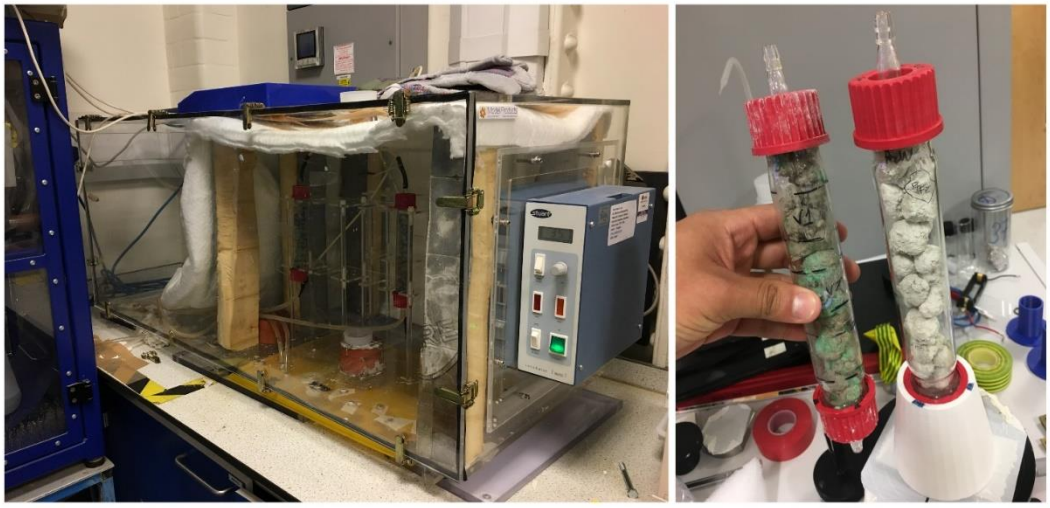

Figure 2. Experimental rig with incubator and columns of agglomerates A (left-hand side column) and B (right-hand side column) after curing and before washing.

2.2. XMT scans

In order to track structural changes, the columns were scanned periodically over the 65 days of curing and after water washing the sample for 5 days (Table 3). The XMT machine used was a Nikon 225H XT at an energy level of 89 kV and exposure time of 2 s, producing a linear image resolution of approximately 17 µm. Table 4 summarizes the XMT conditions used to scan the samples, which allowed for an adequate differentiation between pores, grains, and the rock matrix (Figure 3).

Table 3. Scanning intervals for the curing experiments

	Scanning days							
Recipe A	0	3	10	20	32		65	AW
Recipe B	0	1	4	14	20	30	65	AW

*: samples were washed with water for 5 days immediately after the 65 days of curing and at this point the last XMT images were acquired (AW stands for After Washing).

Table 4. Scanning conditions and settings.

Filament	Tungsten
Energy level (kV)	89
Intensity (µA)	165
Exposure time (s)	2
Number of angular projections	3185
Linear resolution (µm)	17

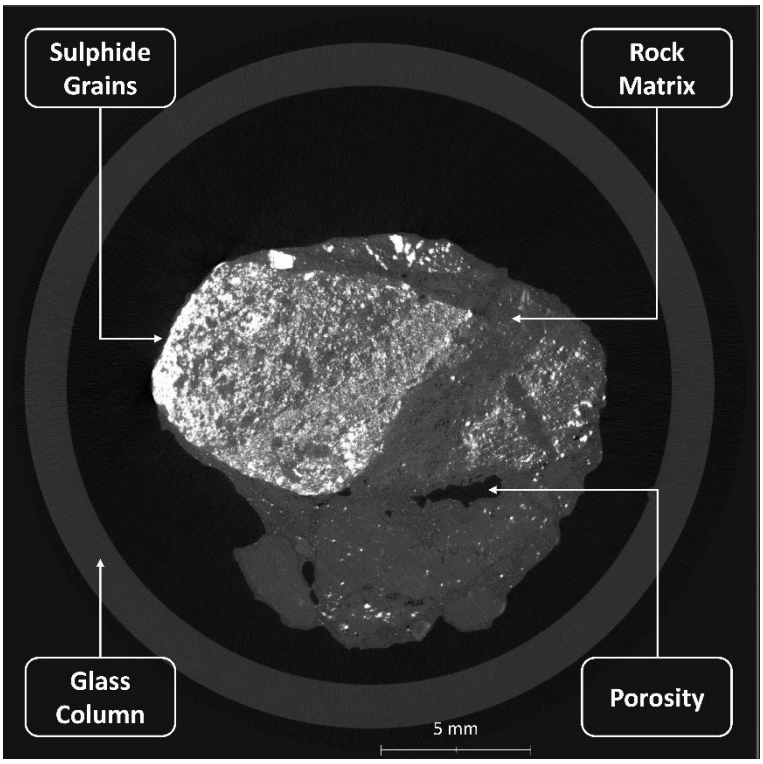

Figure 3. Cross-section of one of the scanned columns showing that it is possible to differentiate sulphide grains, porosity, and rock matrix.

The quantitative tracking of the mineral dissolution and reprecipitation presented a number of challenges. Firstly, the precipitates and the original grains have similar X-ray attenuations, though different enough for them to be segmented from one another with careful thresholding (see section 2.3). The second challenge was to track both the individual agglomerates, as well as the grains within them. While 3D particle and grain tracking has previously been applied to quantification of leaching behaviour (Lin *et al.*, 2016; Reyes *et al.*, 2017), to the authors knowledge, it has not previously been applied to agglomerated ores. Tracking agglomerates across multiple images present additional challenges compared to solid ore particles in that not only can they rotate and translate, but they can also shrink, deform, and break during the curing process.

2.3. Quantification methodology

The methodology presented in this paper is based on the algorithms developed by Lin et al. (2015) and significantly extended to address the morphological changes agglomerated ores undergo. The algorithm also includes an additional step in order that the sulphide grains can be segmented from the precipitated species. The methodology to track chemical and structural changes in agglomerated ores is as follows:

1) Agglomerates are subtracted from the background using the Otsu algorithm (Otsu, 1979) in order to reduce errors associated with signal noise.
2) Each agglomerate is segmented and assigned a unique label by performing a 26-neighbour connectivity analysis. The centroid location of each sample is recorded for further agglomerate tracking.
3) All bright phases are segmented from the rock matrix using the Moments algorithm (Tsai, 1985). A combination of all sulphide compounds (i.e. copper sulphides, pyrite, chloride-sulphides, etc.) is obtained.
4) Sulphide grains are segmented from the combined bright phase (metal containing) material obtained in step 3 by using the Maximum entropy algorithm (Kapur, Sahoo and Wong, 1985). This is possible because precipitates and sulphide grains present slightly different attenuation values under the scanning conditions used (Table 3).

5) A binary mask is obtained for each segmented phase (i.e. sulphides and precipitates). It is important to note that the subsequent image processing is performed on these masks and not the original images in order to avoid adding systematic errors[2].
6) Agglomerates are registered into the reference day using a combination of anisometric and rigid motion transformations, and a transformation matrix is obtained.
7) Using the transformation matrix obtained in step 6, a normalised distance map is produced in order to account for structural changes in further quantifications over the curing process[3].

Once this methodology has been applied to the set of images obtained for the process, a 4D database is produced containing information about volume, location, and concentration of each component. Figure 4 shows a schematic representation of this methodology applied to agglomerates of recipe A at day 30, by which point a large precipitate content had developed. From the figure it can be seen that sulphides and precipitates were successfully segmented and could thus be used as the basis for a quantitative analysis. It is important to note that steps 6 and 7 are not presented in Figure 4 since these produce a time series containing the quantification analyses for the scanned objects as their output.

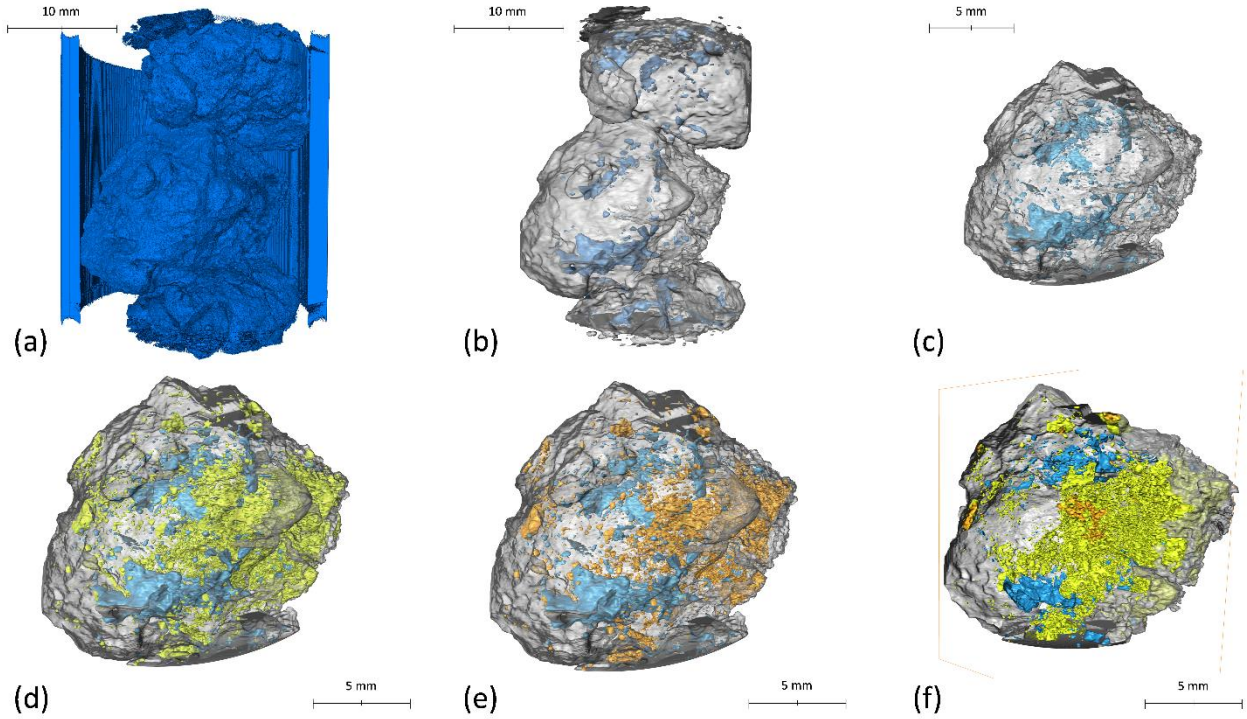

Figure 4. Methodology for quantification of sulphide grains and precipitating species. (a): Agglomerates are subtracted from the background by using the Otsu algorithm (Otsu, 1979); (b): The internal porosity is segmented for further analysis of structural changes; (c) Each agglomerate is segmented, recording the centroid location of each sample (step 2); (d) The bright phases are segmented from the rock matrix by using the Moments algorithm (Tsai, 1985) and a combination of all sulphide compounds (yellow rendering) is obtained (step 3); (e) Sulphide grains are segmented (orange rendering) from the compound combination obtained in (d) by using the Maximum entropy algorithm (Kapur, Sahoo and Wong, 1985) (step 4); (f) A

[2] The interpolation required to project grains from advanced curing stages back onto a grid corresponding to earlier stages will make grain boundaries diffuse. Thus, an error associated with the measured grain volume will be introduced. This error is mitigated by projecting a mask onto the appropriate grid in order to identify the relevant grains and then using the untransformed image to calculate the grain volumes identified using the mask.

[3] After applying the transformation matrix that relates each agglomerate sample with the reference image (i.e. day 0), a distance map is produced. By finding the maximum distance in the map and dividing every single distance value by the maximum value, a normalised version of this map can be obtained. This normalised map will account for any remaining morphological differences between both images, and its values will range from 0 to 1, with 0 being the minimum and 1 the maximum distances to surface.

cross section of the binary mask obtained for each segmented phase (i.e. sulphides and precipitates) is presented as most of the precipitating species cover the initial sulphide grains (step 5).

3. Results

The results presented in this section were obtained for two different columns of agglomerates, each with a different agglomeration recipe as presented in Table 1, with the main aim being to assess the impact of the chloride ions on the sample performance over the curing process. In addition to the 3D time resolved XMT analysis, 2D BSE-MLA analyses were performed on two agglomerates after the curing process in order to obtain more detailed mineralogical information at a higher resolution than that obtained from the XMT.

3.1. Structural changes

In order to carry out preliminary assessments of structural changes directly from the XMT images, a set of cross sections for both agglomerate types at three different times over the curing period as well as after water washing were produced (Figure 5). It can be observed that over the course of the curing stage, agglomerates developed internal cracks. This is probably due to a combination of the formation of mineral compounds due to sulphide dissolution/reprecipitation, as well as to water evaporation occurring over the curing process. Furthermore, agglomerates of recipe A (with chloride ions) contain a large amount of precipitates near the surface, whereas these compounds are virtually absent for agglomerates of type B (without chloride ions). It can also be seen that after water washing the samples, the precipitated species present near the surface of agglomerates of recipe A were largely removed. This is because these precipitates are predominantly soluble metal compounds, which allows them to be redissolved in the presence of the wash water.

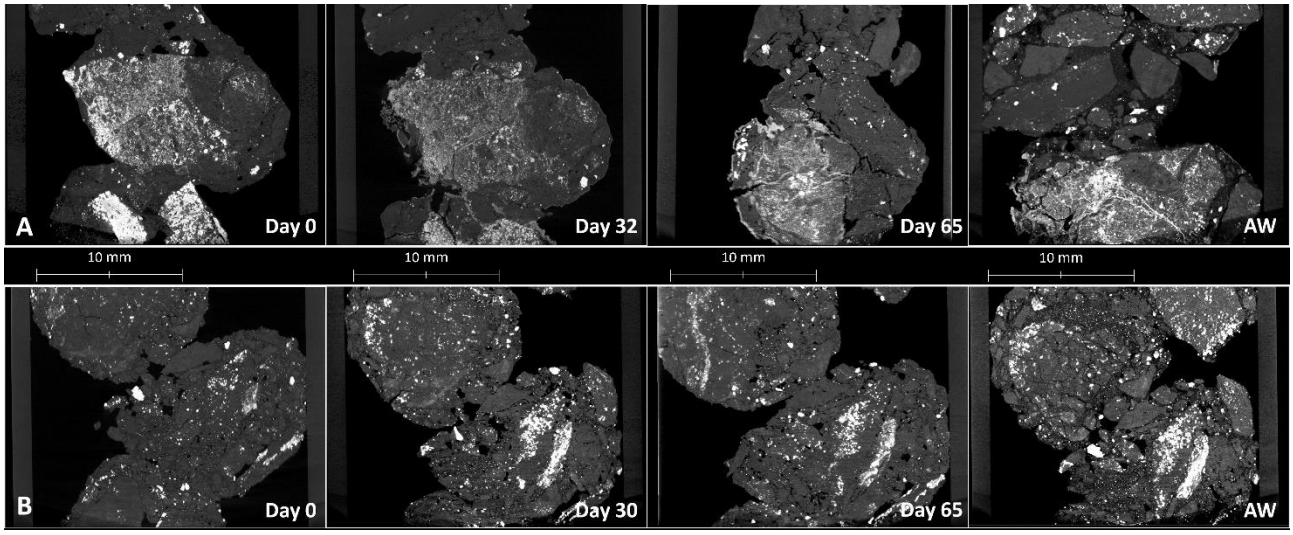

Figure 5. Cross-sections of the XMT images obtained for columns of agglomerates of recipes A and B (with and without NaCl, respectively). On top, agglomerates of recipe A at days 0, 32 and 65 of curing and after washing (AW). On the bottom, agglomerates of recipe B at days 0, 30 and 65 of curing and after washing (AW).

The XMT data can also be used to assess the evolution of the porosity distribution within the agglomerates. This is important for subsequent leach behaviour as this macroscopic internal porosity provides a path for reactants to enter the agglomerates and dissolved metal species to leave. The 3D images of this internal porosity can be obtained using steps 1 and 2 of the methodology explained in section 2.3. Figure 6 shows how the internal porosity develops as the curing proceeds. While both agglomerate types develop internal cracks, which significantly increase the mean internal porosity, agglomerates of recipe B present higher porosity at each timestep assessed. The reduced porosity of agglomerates A relative to those of recipe B can be due to reprecipitation of the previously dissolved species within the pore spaces due to

saturation of solution. There is also a difference in the initial porosity that could either be random, given the small number of agglomerates imaged (6 or 7 agglomerate samples), or actually due to differences in the recipe used to produce the agglomerates.

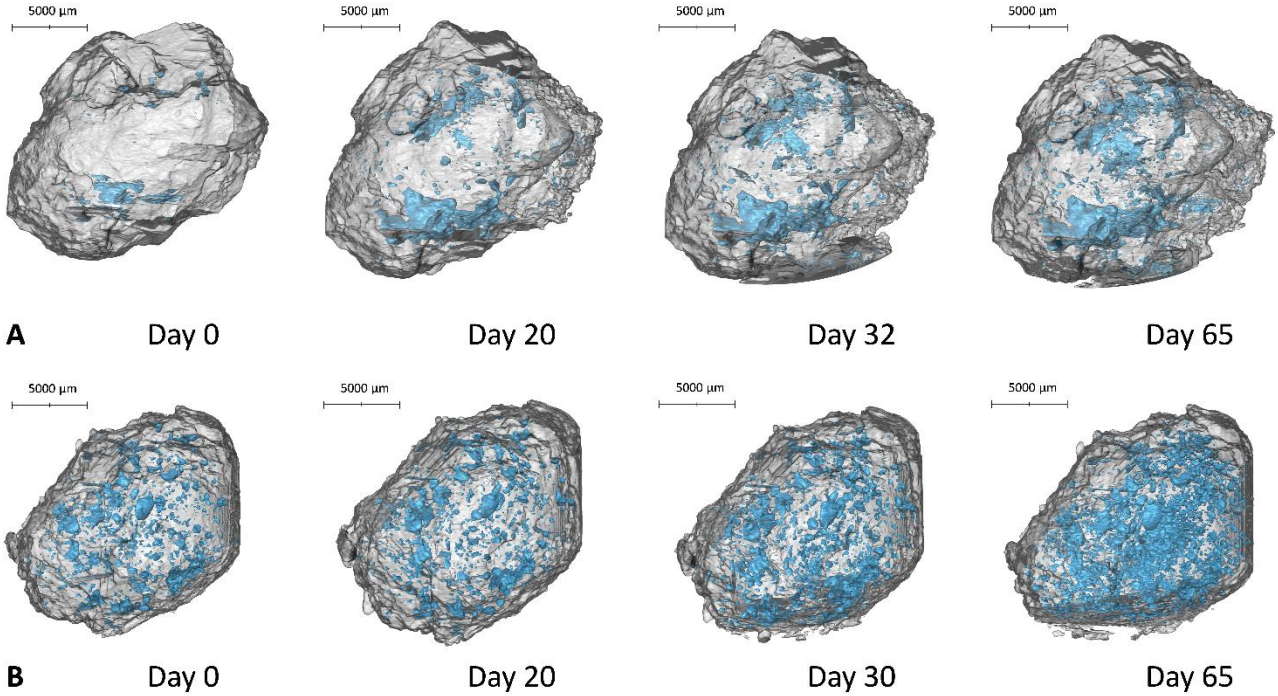

Figure 6. 3D rendering of a single agglomerate of recipes A and B at different curing timesteps. The internal porosity of the agglomerates is presented in light blue, whereas the rock matrix in translucent grey.

Another possible explanation of this difference in porosity is the presence of bridges that bind particles over the curing process. These bridges are a product of the dissolution and reprecipitation of species, and they are responsible for providing the agglomerates with the mechanical stability and strength necessary for the subsequent heap leaching stage. Thus, even though the porosity may be lower for samples of recipe A, this might only be a result of a greater number of bridges forming. Although mechanical stability tests, such as compression and soak tests, are essential in order to assess the mechanical stability of agglomerates, such an analysis was out of the scope of this study.

3.2. Energy-dispersive X-rays analysis with Scanning Electron Microscope for mineral identification.

With the purpose of identifying the precipitating species that formed over the 65 days of curing, two unwashed agglomerates of recipe A were sectioned and polished. These sections were selected in order to expose a surface that contained mineralogical information that was representative of what was present in the cured agglomerates. The samples were imaged using EDX/SEM, obtaining a set of Backscatter Electron (BSE) images. Further quantification was achieved using the Mineral Liberation Analyzer (MLA) automated system. Figure 7 presents the MLA results obtained with the main mineral components highlighted. From the figure it is possible to identify a set of copper-chloride compounds that have precipitated over both the agglomerate surface and the internal pores. Also, a close-up view of a region containing large quantities of these compounds are shown in a red rectangle for Figure 7.A, and in a blue rectangle for Figure 7.B. Since these are Cu-S-Cl-O complexes[4] of unknown chemical structure, they are named by their mineralogical occurrence. The elemental composition of each complex, as well as their fraction by weight of the sample,

[4] The Illite- and Kaolinte-containing species are intimately associated with the host minerals such that the interaction volume of the measurement spot could not completely separate them from the Cu-Cl-S complexes.

are further described in Table 5. These complexes represent a high fraction by weight of the metal containing species within the sample, which is consistent with the observations from Figure 5.

Another interesting result is the presence of a copper-sulphide compound that grows from the chalcopyrite grains as needle-shaped crystals. This compound is probably a product of grain dissolution and instant reprecipitation, suggesting that the precipitation timescales might be different depending on the location of the grains within the agglomerate's structure. Figure 8 shows these crystals and the main elemental components.

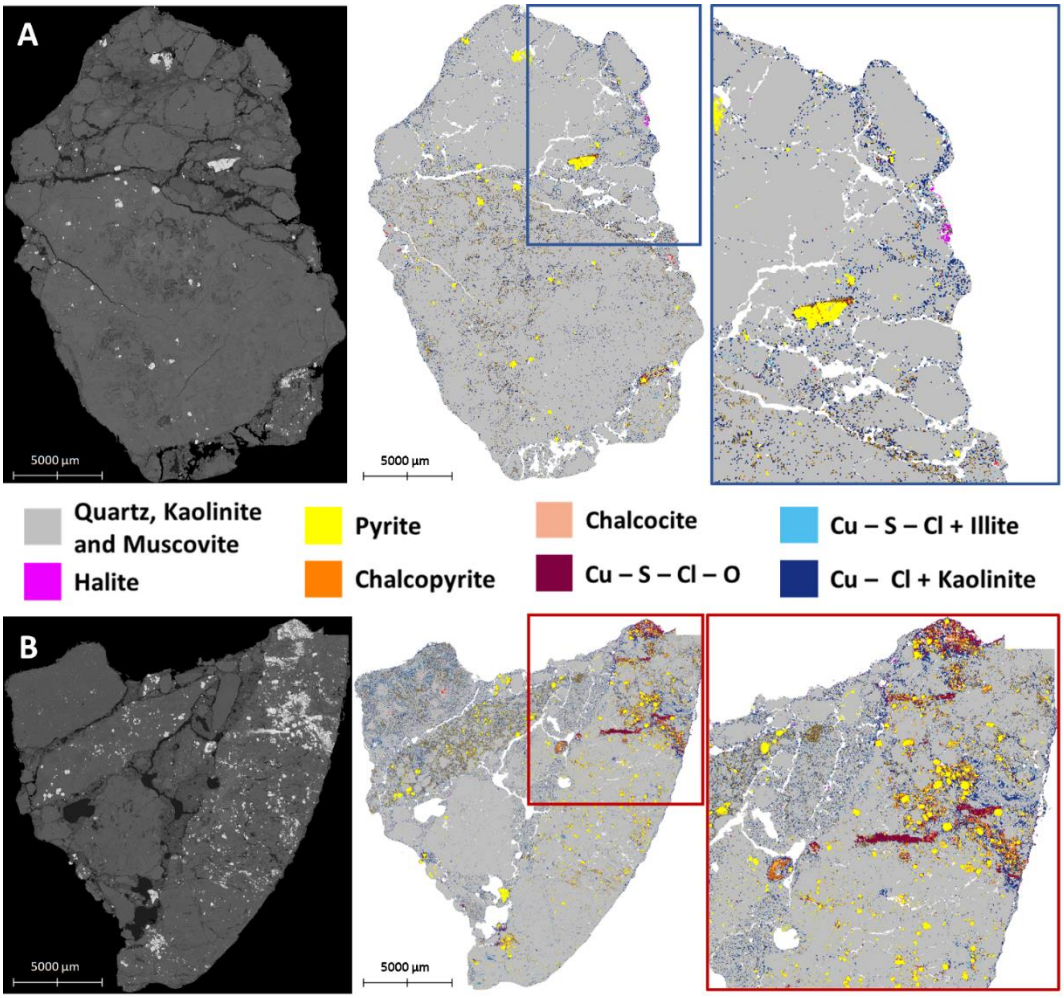

Figure 7. MLA results for two agglomerates of recipe A (containing 150 g/t of NaCl) after 65 days of curing. A: Agglomerate with high formation of the Cu – Cl – Kaolinite compound. The BSE image obtained from SEM is shown on the left, whereas the MLA is shown in the middle with a blue box, which is a close-up view of the precipitated material on the agglomerate surface. B: Agglomerate with high formation of the Cu – S – Cl – O complex. The BSE image obtained from SEM is shown on the left, whereas the MLA is shown in the middle with a red box, which is a close-up view of this compound precipitated in the internal pores and close to the agglomerate surface.

Table 5. Composition by weight of the copper-chloride complexes formed at day 65 of curing, as well as their fraction by weight of the sample.

	Composition by weight (%)							Fraction of the sample by weight (%)
	Cu	**S**	**Cl**	**O**	**Si**	**Al**	**Fe**	
Cu – S – Cl – O	44.6	15.1	10.8	18.3	0.5	0.7	8.1	0.6
Cu – S – Cl + Illite	3.1	2.0	1.4	44.6	24.1	24.4	0.4	0.7
Cu – Cl + Kaolinite	53.1	-	12.5	19.9	7.0	7.5	-	11.7

(this information corresponds to the mineral map presented in Figure 7)

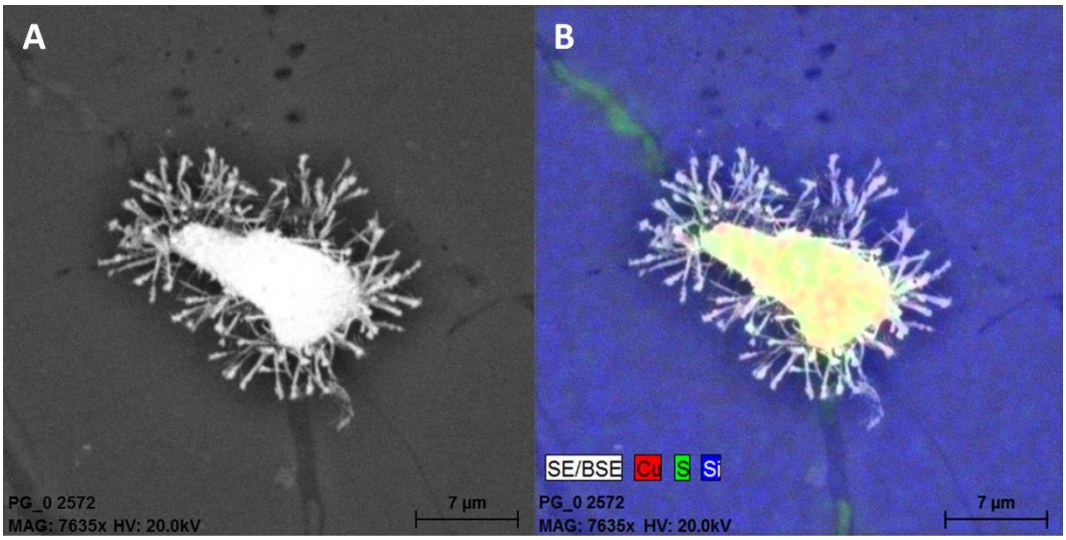

Figure 8. Copper-sulphide grain leached and reprecipitated after 65 days or curing. A: grayscale image; and B: elemental composition of the needle-shaped crystals that form as a product of the curing process.

3.3. Sulphide distribution over the curing process

Since the agglomeration solution includes acid, ferric, cupric, and chloride ions, a degree of leaching is expected to occur over the curing process (section 1.1). The analysis of this leaching is complicated by the fact that all the dissolved metals will remain in the agglomerates as there is no solution flowing through the columns, as it would be the case in a more conventional leach test. Metals can only change their mineralogical occurrence and precipitates are expected to form. There is thus no metal extraction during this process and the overall metal grade must remain approximately constant. Overall, it is therefore expected that the metal sulphide grains will shrink, though some of them may appear to grow as chloride and/or sulphate precipitates form on their surface, while in other regions completely new precipitate grains may form.

Using the segmentation algorithm outlined in section 2.3, the overall metal containing mineral grain volume can be obtained as a function of distance from the agglomerate surface at different times for both recipes (Figure 9). Since the leaching solution is introduced into the agglomerates during the agglomeration process, leaching is expected to occur everywhere within the agglomerates. On the other hand, water evaporation will occur predominantly from the agglomerate surface, which means that metal ion concentration in solution will increase towards the surface promoting precipitation in these areas.

It is also possible to observe that a period of 20 days was the minimum curing time necessary to obtain an appreciable extent of overall sulphide dissolution for agglomerates of recipe A, whereas for agglomerates

of recipe B there is no significant dissolution over the entire 65 days of curing. It should be stressed that Figure 9 shows the change in the total volume of metal ion containing species. The yellow and red sections correspond to agglomerate regions where the precipitation reactions are mainly occurring, and this precipitate formation is represented as volume growth when a more basic segmentation method is used (as in this case). Yet, in order to quantify the two processes occurring in these regions (i.e. grain dissolution and reprecipitation of species), a more detailed description is required, which can be obtained by assessing the extent of sulphide dissolution, separately from the precipitation of species.

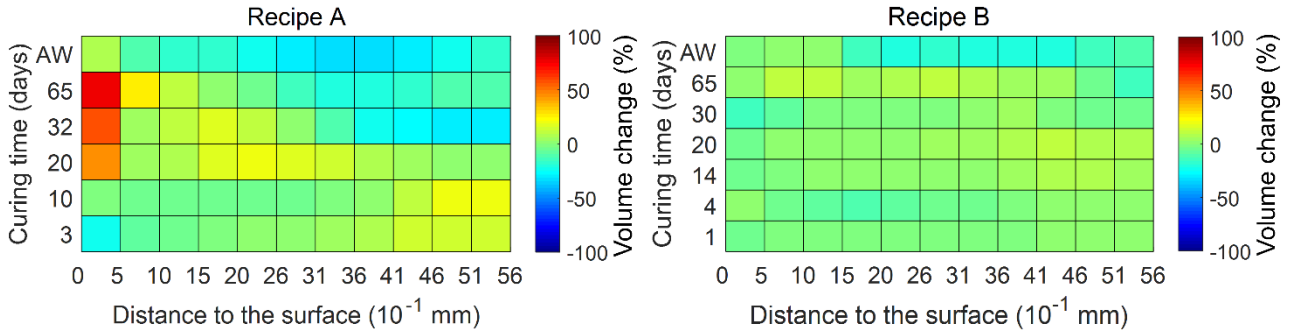

Figure 9. Volume change of the metal-containing grains measured after 65 days of curing and 5 days of water washing the samples. Sample A (left) shows a higher overall leaching extent, and particularly high in areas far from the surface. This is not the case for sample B (right).

3.4. Leaching extent over the curing process

Using the more advanced segmentation methodology explained earlier (section 2.3), it is possible to analyse the mean concentration of species. The samples contain different sulphide grades due to their natural occurrence. Thus, in order to obtain comparable results, the mean concentration was normalised by dividing the value at each scanning point by the initial sulphide concentration. The normalised concentration of species i, C_i', can be obtained as follows:

$$C_i' = \frac{C_i}{C_{species_0}} \tag{3}$$

where C_i is the concentration of species i (e.g. sulphide grains (MS), precipitates (precip), or the overall metal ion containing species (species)); and $C_{species_0}$ is the initial concentration of sulphide species.

Figure 10 shows the normalised concentration for each sample. As expected, there is a substantial leaching occurring for the samples agglomerated using NaCl as an additive (recipe A), whereas agglomerates of recipe B show virtually no leaching occurring after agglomeration (i.e. day 0). Another interesting result is the amount of species that were removed after the water wash, with approximately 50% of the initial sulphides being removed from agglomerates of recipe A, and only around 20% of species removed from samples of recipe B. Lastly, as it was possible to quantify precipitate formation, the trends show that even though these species form more rapidly in samples without chloride ions (approximately 15% of species are precipitates, which are present throughout the curing process), there is no further formation of these compounds after the first contact with solution, meaning that leaching virtually stopped after that which occurred during the agglomeration. This is not the case for samples where chloride ions are present, as species continue to precipitate even at later stages, reaching a concentration of approximately 48% of the overall sulphide species at day 65 of curing.

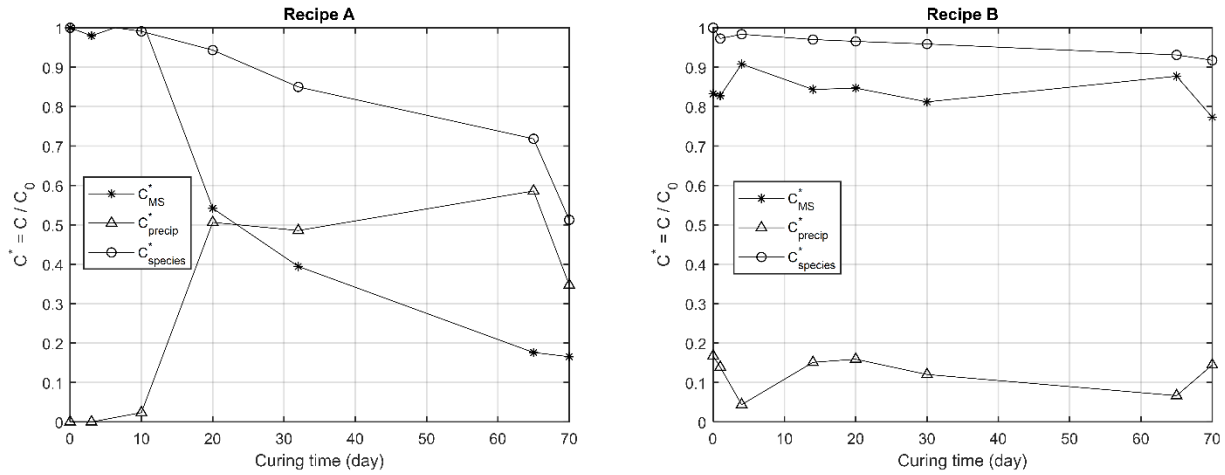

Figure 10. Normalised concentration of species at different stages of the curing process, and after water washing the samples.

Since the volume and distance to surface of both sulphide grains and precipitates were successfully quantified and recorded, it is also possible to describe in more detail the spatial distribution of species within the sample. An important point to stress, though, is that this methodology can only quantify volume. Thus, it is convenient to define the dimensionless concentration of species i, C_i^*, by considering the density of each component:

$$C_i^* = \frac{C_i}{\rho_i} \tag{4}$$

where ρ_i is the mass density of species i (e.g. sulphide grains (MS), precipitates (precip), or the overall sulphide species).

This dimensionless concentration can be obtained directly by using this quantification methodology. It can then be plotted as a function of distance to the nearest surface, giving a better idea of the chemical changes occurring throughout the agglomerate structure. Figure 11 shows this plot for the sulphide grains, and Figure 12 shows it for the precipitating species.

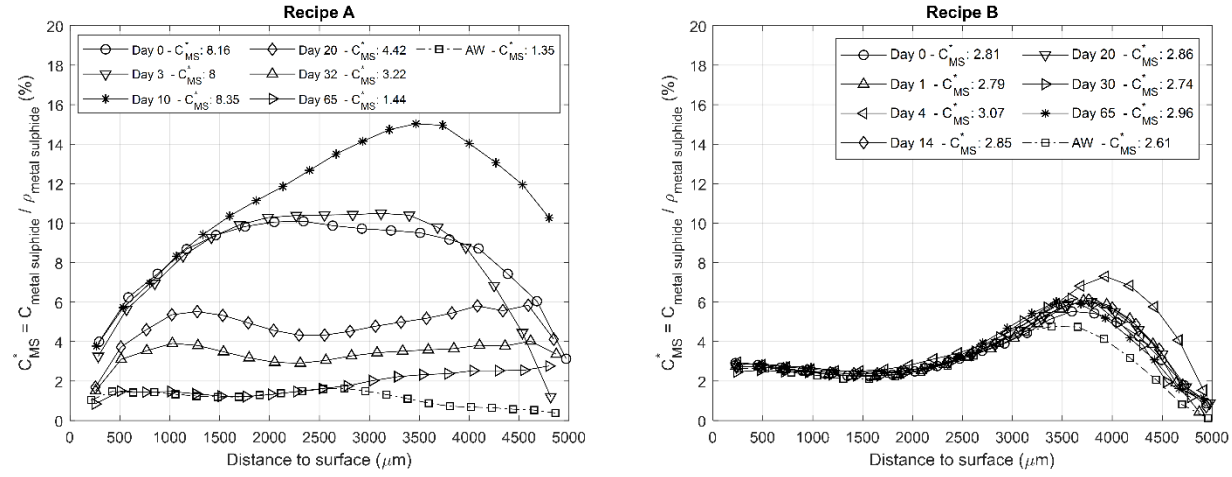

Figure 11. Dimensionless concentration of sulphide grains as a function of distance to the nearest surface.

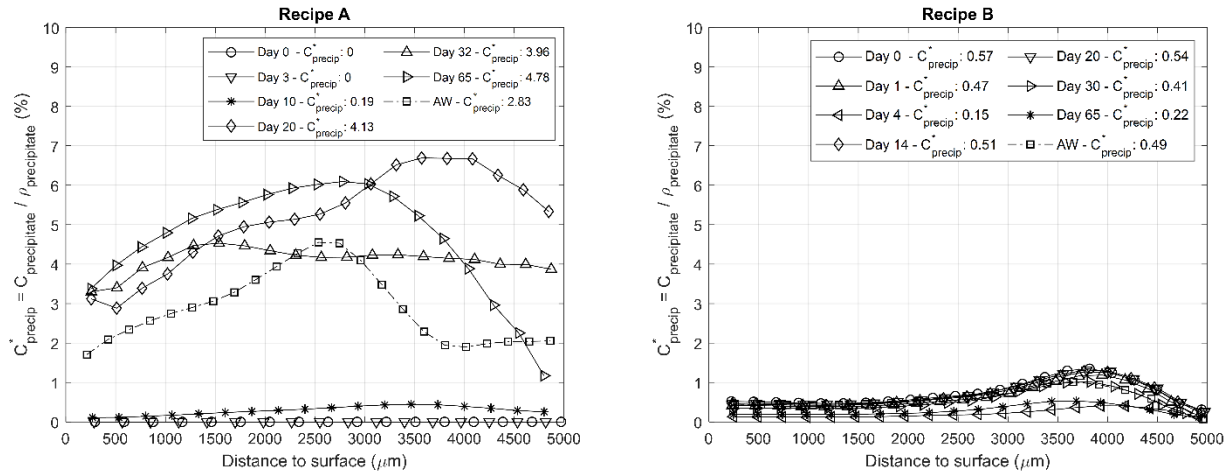

Figure 12. Dimensionless concentration of precipitates as a function of distance to the nearest surface.

As there is no clear trend from the figures, it becomes convenient to define another dimensionless quantity that we called the Precipitation Ratio (PR). Considering that precipitates can only form once the initial sulphide grains have been dissolved, this PR can be defined as the amount of precipitates formed at a certain timestep w.r.t the amount of sulphide grains remaining at the point:

$$PR = \frac{C^*_{precipitate}}{C^*_{Metal\ Sulphide}} \tag{5}$$

Bearing in mind that the forming precipitates are water-soluble species (Figure 9), this PR will be a strong indicator of the proportion of sulphide species that will be easily leached out when the subsequent leaching process starts.

For instance, a PR of more than 1 will mean that at a certain point of distance and time, there will be more precipitates than sulphide grains within the agglomerate. On the other hand, a PR of values closer to 0 will indicate that there is virtually no leaching occurring over the curing process, and either longer times or additional reagents are necessary to achieve a higher leaching extent over the curing of agglomerated ores.

Figure 13 shows the PR values as a function of distance to the nearest distance for both sample types. It is also possible to observe that as the agglomerates dried out, the reprecipitation of metal species occurred especially close to the agglomerate surface. These results are consistent with what was observed from both the preliminary assessment of structural changes and the MLA analyses (sections 3.1. and 3.2, respectively).

The reason why the precipitation will occur mainly near the agglomerate surface is because the evaporation will occur mainly from near the outer surface, which will induce an outward flow of liquid within the agglomerate and higher concentration of soluble species towards the edge of the agglomerates.

Figure 13 also shows that the mean PR value for agglomerates of recipe A at day 20 is approximately 1, so there is virtually the same concentration of remaining sulphide grains as there is of precipitates. This is consistent with the preliminary observations from the more basic analysis in section 3.3, reaffirming that 20 days would be the minimum curing time in presence of chloride ions to obtain meaningful results. This is not the case for agglomerates of recipe B, as their PR values never reach values over 0.20, which indicates a very low reprecipitation pattern and, thus, practically no appreciable dissolution extent over the 65 days of curing assessed.

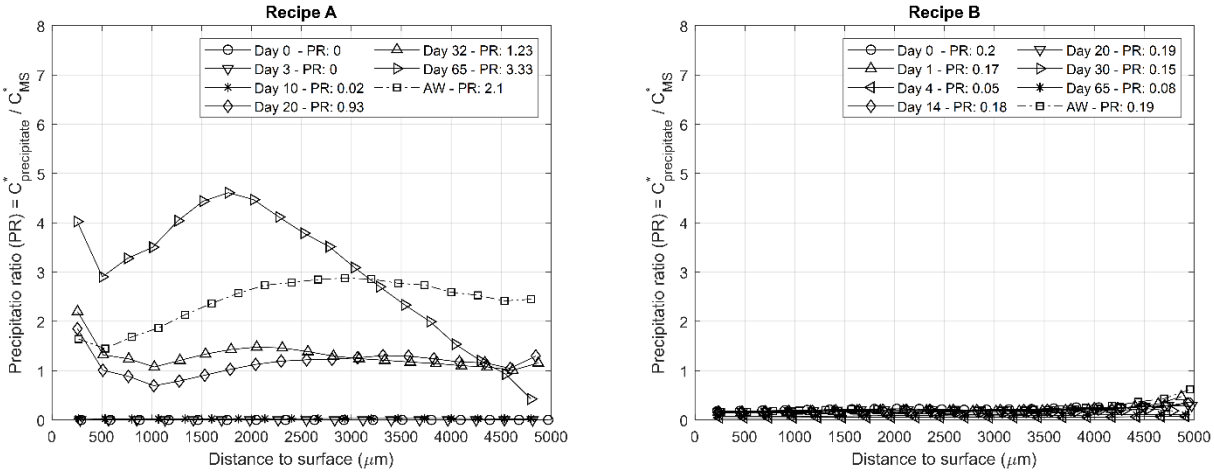

Figure 13. Precipitation Ratio (PR) as a function of distance to the nearest surface.

4. Conclusions

A study of an extended curing process for copper-sulphide ore agglomerates was successfully performed. This included the development of a methodology for tracking the performance of the agglomerated ores and, in particular, a tool for quantifying grain scale leaching extent over the curing process. Due to the non-destructive and non-invasive nature of XMT scans, it was possible to successfully track the grain scale volume evolution over the curing process, and separately quantify the grain dissolution extent from the precipitation of species.

The study showed that curing mineral samples in the presence of chloride ions made a significant difference to the agglomerate structure and the dissolution rate of sulphides. The assessment of influence of curing period time on this leach performance show that for the agglomerates containing NaCl, most of the leaching occurs within the first 20 days of curing, indicating that this may be the appropriate curing length to use, though the time evolution of other agglomerate properties such as the mechanical stability and strength of the material are still being assessed.

Furthermore, approximately 50% of the precipitates (which are mainly formed by the dissolved metals that reprecipitated as complex species of different mineralogy due to solution saturation) were water washed for samples agglomerated with addition of chloride ions, whereas only a 20% when using a more typical agglomeration solution (i.e. containing no chloride ions). This result suggests that precipitating species are water soluble and that a high concentration of chloride ions in the agglomeration solution enhances metal dissolution over the curing process. Thus, it is an effective chemical alternative to bioleaching for sulphide ores.

5. Acknowledgements

The authors would like to acknowledge the Electrochemical Innovation Lab (EIL) at the University College London for their help with the XMT scans, the Nanoscale and Microscale Research Centre (nmRC) at the University of Nottingham for performing the BSE-MLA analyses, and Clement Chibwana for his advice on chalcopyrite agglomeration and leaching in presence of chloride ions. The authors would also like to acknowledge the Becas Chile program of the Agencia Nacional de Investigación y Desarrollo (ANID) and the Institute of Materials, Minerals, and Mining (IOM3) for their funding during this project.

6. Bibliography

Bobadilla-Fazzini, R. A., Pérez, A., Gautier, V., Jordan, H., Parada, P. (2017) 'Primary copper sulfides bioleaching vs. chloride leaching: Advantages and drawbacks', *Hydrometallurgy*, 168, pp. 26–31. doi: 10.1016/j.hydromet.2016.08.008.

Carneiro, M. F. C. and Leão, V. A. (2007) 'The role of sodium chloride on surface properties of chalcopyrite leached with ferric sulphate', *Hydrometallurgy*. Elsevier, 87(3–4), pp. 73–82. doi: 10.1016/J.HYDROMET.2007.01.005.

Cerda, C. P., Taboada, M. E., Jamett, N. E, Ghorbani, Y., Hernández, P. C. (2018) 'Effect of Pretreatment on Leaching Primary Copper Sulfide in Acid-Chloride Media', pp. 1–14. doi: 10.3390/min8010001.

Dobson, K. J., Harrison, S. T.L., Lin, Q., Bhreasail, A. N., Fagan-Endres, M. A., Neethling, S. J., Lee, P. D., Cilliers, J. J.(2017) 'Insights into ferric leaching of low grade metal sulfide-containing ores in an unsaturated ore bed using X-ray computed tomography', *Minerals*, 7(5), pp. 1–16. doi: 10.3390/min7050085.

Garcia, D., Lin, C. L. and Miller, J. D. (2009) 'Quantitative analysis of grain boundary fracture in the breakage of single multiphase particles using X-ray microtomography procedures', *Minerals Engineering*. Elsevier Ltd, 22(3), pp. 236–243. doi: 10.1016/j.mineng.2008.07.005.

Gay, S. L. and Morrison, R. D. (2006) 'Using Two Dimensional Sectional Distributions to Infer Three Dimensional Volumetric Distributions – Validation using Tomography', 23, pp. 246–253. doi: 10.1002/ppsc.200601056.

Ghorbani, Y., Franzidis, J. P. and Petersen, J. (2016) 'Heap leaching technology - Current State, innovations, and future directions: A review', *Mineral Processing and Extractive Metallurgy Review*. Taylor & Francis, 37(2), pp. 73–119. doi: 10.1080/08827508.2015.1115990.

Hernández, P. C., Dupont, J., Herreros, O. O., Jimenez, Y. P., Torres, C. M.(2019) 'Accelerating copper leaching from sulfide ores in acid-nitrate-chloride media using agglomeration and curing as pretreatment', *Minerals*, 9(4), pp. 1–13. doi: 10.3390/MIN9040250.

Kapur, J. N., Sahoo, P. K. and Wong, A. K. C. (1985) 'A new method for gray-level picture thresholding using the entropy of the histogram.', *Computer Vision, Graphics, & Image Processing*, 29(3), pp. 273–285. doi: 10.1016/0734-189X(85)90125-2.

Kareh, K. M., Lee, P. D., Atwood, R. C., Connolley, T., Gourlay, C. M.(2014) 'Revealing the micromechanisms behind semi-solid metal deformation with time-resolved X-ray tomography', *Nature Communications*. Nature Publishing Group, 5, pp. 1–7. doi: 10.1038/ncomms5464.

Liddicoat, J. and Dreisinger, D. (2007) 'Chloride leaching of chalcopyrite', *Hydrometallurgy*, 89(3–4), pp. 323–331. doi: 10.1016/j.hydromet.2007.08.004.

Lin, Q., Neethling, S. J., Dobson, K. J., Courtois, L., Lee, P. D.(2015) 'Quantifying and minimising systematic and random errors in X-ray micro-tomography based volume measurements', *Computers and Geosciences*. doi: 10.1016/j.cageo.2014.12.008.

Lin, Q. (2015) 'Use of X-ray Computed Microtomography to Measure the Leaching Behaviour of Metal Sulphide Ores', (February).

Lin, Q., Barker, D. J., Dobson, K. J., Lee, P. D., Neethling, S. J.(2016) 'Modelling particle scale leach kinetics based on X-ray computed micro-tomography images', *Hydrometallurgy*. The Authors, 162, pp. 25–36. doi: 10.1016/j.hydromet.2016.02.008.

Lin, Q., Neethling, S. J., Courtois, L., Dobson, K. J., Lee, P. D.(2016) 'Multi-scale quantification of leaching performance using X-ray tomography', *Hydrometallurgy*. doi: 10.1016/j.hydromet.2016.06.020.

Lu, J., Dreisinger, D. and West-Sells, P. (2017) 'Acid curing and agglomeration for heap leaching', *Hydrometallurgy*. Elsevier B.V., 167, pp. 30–35. doi: 10.1016/j.hydromet.2016.10.019.

Lu, Z. Y., Jeffrey, M. I. and Lawson, F. (2000a) 'Effect of chloride ions on the dissolution of chalcopyrite in acidic solutions', *Hydrometallurgy*. doi: 10.1016/S0304-386X(00)00075-X.

Lu, Z. Y., Jeffrey, M. I. and Lawson, F. (2000b) 'Electrochemical study of the effect of chloride ions on the

dissolution of chalcopyrite in acidic solutions', *Hydrometallurgy*. doi: 10.1016/S0304-386X(00)00068-2.

Salinas, K. E., Herreros, O., Torres, C. M. (2018) 'Leaching of Primary Copper Sulfide Ore', (i), pp. 1–12. doi: 10.3390/min8080312.

Miller, J. D., Lin, C. L., Hupka, L., Al-Wakeel, M. I. (2009) 'Liberation-limited grade/recovery curves from X-ray micro CT analysis of feed material for the evaluation of separation efficiency', *International Journal of Mineral Processing*. Elsevier B.V., 93(1), pp. 48–53. doi: 10.1016/j.minpro.2009.05.009.

Nicol, M., Miki, H. and Velásquez-Yévenes, L. (2010) 'The dissolution of chalcopyrite in chloride solutions: Part 3. Mechanisms', *Hydrometallurgy*. Elsevier B.V., 103(1–4), pp. 86–95. doi: 10.1016/j.hydromet.2010.03.003.

Otsu, N. (1979) 'A threshold selection method from gray-level histograms.', C(1), pp. 62–66. doi: 10.1109/TSMC.1979.4310076.

Purkiss, S. and Anthony, R. (2004) 'Heap leaching base metals from oxide ores' (WO/2004/031422).

Quezada, V., Velásquez, L., Roca, A., Benavente, O., Melo, E., Keith, B. (2018) 'Effect of curing time on the dissolution of a secondary copper sulphide ore using alternative water resources', *IOP Conference Series: Materials Science and Engineering*, 427(1). doi: 10.1088/1757-899X/427/1/012030.

Ram, R., Beiza, L., Becker, M., Pownceby, M. I., Chen, M., Yang, Y., Yang, S., Petersen, J. (2020) 'Study of the leaching and pore evolution in large particles of a sulfide ore', *Hydrometallurgy*. Elsevier, 192(October 2019), p. 105261. doi: 10.1016/j.hydromet.2020.105261.

Reyes, F., Lin, Q., Udoudo, O., Dodds, C., Lee, P. D., Neethling, S. J. (2017) 'Calibrated X-ray micro-tomography for mineral ore quantification', *Minerals Engineering*, 110(May), pp. 122–130. doi: 10.1016/j.mineng.2017.04.015.

Reyes, F., Lin, Q., Cilliers, J.J., Neethling, S.J. (2018) 'Quantifying mineral liberation by particle grade and surface exposure using X-ray microCT', *Minerals Engineering*, 125, pp. 75–82. doi: 10.1016/j.mineng.2018.05.028.

Tsai, W. H. (1985) 'Moment-preserving thresholding: a new approach.', *Computer Vision, Graphics, & Image Processing*, 29(3), pp. 377–393. doi: 10.1016/0734-189x(85)90133-1.

Velásquez-Yévenes, L., Torres, D. and Toro, N. (2018) 'Leaching of chalcopyrite ore agglomerated with high chloride concentration and high curing periods', *Hydrometallurgy*. doi: 10.1016/j.hydromet.2018.10.004.

Veloso, T. C., Peixoto, J. J M., Pereira, M. S., Leao, V. A. (2016) 'Kinetics of chalcopyrite leaching in either ferric sulphate or cupric sulphate media in the presence of NaCl', *International Journal of Mineral Processing*. Elsevier B.V., 148, pp. 147–154. doi: 10.1016/j.minpro.2016.01.014.

Yang, Y., Yang, Y., Gao, X., Petersen, J., Chen, M. (2019) 'Microstructure evolution of low-grade chalcopyrite ores in chloride leaching - A synchrotron-based X-ray CT approach combined with a data-constrained modelling (DCM)', *Hydrometallurgy*. Elsevier, 188(April), pp. 1–13. doi: 10.1016/j.hydromet.2019.06.004.

Yévenes, L. V., Miki, H. and Nicol, M. (2010) 'The dissolution of chalcopyrite in chloride solutions', *Hydrometallurgy*. Elsevier B.V., 103(1–4), pp. 80–85. doi: 10.1016/j.hydromet.2010.03.004.

Yoo, K., Soo-kyung, K., Jae-chun, L., Ito, M., Masami, T., Naoki, H. (2010) 'Effect of chloride ions on leaching rate of chalcopyrite', *Minerals Engineering*. Elsevier Ltd, 23(6), pp. 471–477. doi: 10.1016/j.mineng.2009.11.007.